Research Article Vol. 5, No. 3 / March 2018 / Optica 257

Compact gain-saturated x-ray lasers down to 6.85 nm and amplification down to 5.85 nm

Alex Rockwood,[1] Yong Wang,[2] Shoujun Wang,[2] Mark Berrill,[2,3] Vyacheslav N. Shlyaptsev,[2] and Jorge J. Rocca[1,2,*]

[1]Physics Department, Colorado State University, Fort Collins, Colorado 80523, USA
[2]Electrical and Computer Engineering Department, Colorado State University, Fort Collins, Colorado 80523, USA
[3]Oak Ridge National Laboratory, Oak Ridge, Tennessee 37831, USA
*Corresponding author: jorge.rocca@colostate.edu

Received 24 November 2017; revised 9 February 2018; accepted 9 February 2018 (Doc. ID 314151); published 2 March 2018

Plasma-based x-ray lasers allow single-shot nano-scale imaging and other experiments requiring a large number of photons per pulse to be conducted in compact facilities. However, compact repetitively fired gain-saturated x-ray lasers have been limited to wavelengths above $\lambda = 8.85$ nm. Here we extend their range to $\lambda = 6.85$ nm by transient traveling wave excitation of Ni-like Gd ions in a plasma created with an optimized pre-pulse followed by rapid heating with an intense sub-picosecond pump pulse. Isoelectronic scaling also produced strong lasing at 6.67 nm and 6.11 nm in Ni-like Tb and amplification at 6.41 nm and 5.85 nm in Ni-like Dy. This scaling to shorter wavelengths was obtained by progressively increasing the pump pulse grazing incidence angle to access increased plasma densities. We experimentally demonstrate that the optimum grazing incidence angle increases linearly with atomic number from 17 deg for $Z = 42$ (Mo) to 43 deg for $Z = 66$ (Dy). The results will enable applications of sub-7 nm lasers at compact facilities.

OCIS codes: (140.0140) Lasers and laser optics; (140.7240) UV, EUV, and X-ray lasers; (340.7480) X-rays, soft x-rays, extreme ultraviolet (EUV).

https://doi.org/10.1364/OPTICA.5.000257

1. INTRODUCTION

The need for bright, energetic ultrafast x-ray laser pulses has motivated the commissioning of x-ray free electron lasers [1]. Alternatively, plasma-based x-ray lasers allow many experiments requiring bright, high energy, x-ray laser pulses to be conducted in compact facilities [2–6]. These lasers provide extremely monochromatic radiation, typically $\Delta\lambda/\lambda = 3 \times 10^{-5}$ [7], and when injection-seeded, they can reach full spatial and temporal coherence [8–10]. The efficient generation of high energy x-ray laser pulses requires operation in the gain-saturated regime. In this regime, stimulated emission can extract the majority of the energy stored in the population inversion [11]. Gain saturation in plasma-based x-ray lasers was demonstrated for wavelengths as short as 5.8 nm at large laser facilities [12,13]. However, these results required pump pulse energies on target larger than 70 J, which limited the repetition rate to a few shots per hour. Alternatively, transient table-top lasers [14,15] pumped by picosecond laser pulses at grazing incidence [16,17] require much less energy and can operate at repetition rates of typically 5–10 Hz at wavelengths as short as 10.9 nm [18]. The repetition rate of these lasers was recently increased to 100 Hz using pump lasers pumped by laser diodes [19], and 400 Hz operation was very recently reported at $\lambda = 18.9$ nm in Ni-like Mo [20]. However, the extension of practical plasma-based x-ray lasers that can fire repetitively to sub-10 nm wavelengths is challenging. Alessi *et al.* used laser pump pulse energies of up to 7.5 J on target to extend table-top, repetitive 1 Hz transient collisional soft x-ray amplification down to 7.36 nm [21]. Nevertheless, gain-saturated operation was limited to a shortest wavelength of 8.85 nm in Ni-like La. A more recent experiment conducted in Ni-like Sm using a Nd:glass pump laser capable of firing a shot every 25 min was reported to approach gain saturation [22]. However, this could not be verified due to large pulse-to-pulse output pulse energy variations and the low repetition rate of the pump laser. In the case of the 6.85 nm line of Ni-like Gd, gain was observed in a plasma pumped by 250 J pulses, but the amplification was far from reaching gain saturation [23]. Alternatively, collisional recombination is being explored as a population inversion mechanism for transitions to the ground state to extend table-top lasers to shorter wavelengths [24].

Here we report the extension of gain-saturated compact repetitive x-ray lasers down to 6.85 nm (181 eV) in Ni-like Gd. Furthermore, in the same experiments, we observed gain at even shorter wavelength transitions, down to 5.85 nm (212 eV) in Ni-like Dy. The experiments were performed with a pump laser capable of firing at repetition rates up to 3.3 Hz [25]. We also report measurements of the optimum grazing incidence pumping angle necessary for lasing at these wavelengths. The results

reported here, in combination with previous measurements of the optimum angles for lasing in lower Z ions, allowed us to experimentally determine the optimum pump angle for laser operation at wavelengths between 18.9 nm and 5.85 nm. The results can be used to predict the optimum angles that will be required for lasing at shorter wavelengths.

2. EXPERIMENTAL SETUP AND METHODS

The x-ray lasers were excited irradiating 1–2 mm thick solid slab targets with a sequence of two laser pulses from a $\lambda = 800$ nm chirped pulse amplification Titanium:Sapphire (Ti:Sa) laser. The two-pulse sequence consisted of a normal-incidence pre-pulse that ionizes the plasma to the vicinity of the Ni-like ionization stage, followed by a sub-picosecond pulse impinging at grazing incidence that rapidly heats the electrons to produce a transient population inversion by collisionally electron impact excitation. The sub-picosecond pulse has a grazing incident angle of 35 deg or 43 deg for Sm and Gd, respectively, with a traveling-wave excitation velocity of $(1.0 \pm 0.03)c$. The pump laser has five Ti:Sa stages of amplification, of which the last three are pumped with the frequency-doubled output of high-energy Nd:glass slab amplifiers that we have operated at repetition rates of up to 3.3 Hz [25]. An acousto-optic programmable dispersive filter was used after the laser oscillator to tailor the bandwidth of the laser. This gives us the ability to adjust the length of the uncompressed pre-pulse from 45 ps to 300 ps to find the optimal conditions for laser amplification, which proved critical to obtain the results discussed below. Also, the intensity ratio of the pre-pulse to the sub-picosecond pulse was optimized using different beam splitters deflecting 30%, 40%, or 50% of the beam to be used as the pre-pulse. Optimum pre-pulse plasma conditions were obtained using a 30% and 40% beam splitter to generate a pre-pulse with intensities of $I \sim 1.7 \times 10^{13}$ W cm^{-2} and 2.5×10^{13} W cm^{-2} for Sm and Gd, respectively, with 185 ps duration. The pre-pulse was focused onto the target using the combination of a spherical and a cylindrical lens to form a line focus of approximately 15 μm full width at half-maximum (FWHM) and 9 mm or 10 mm length for Sm and Gd respectively. To achieve efficient pumping by the sub-picosecond pulse, we developed a focusing geometry designed to create a plasma column of constant width along the target. This focusing method, consisting of two cylindrical mirrors, is the same we used previously to obtain gain-saturated lasing in Ni-like La at 8.85 nm [22]. The plasma created by the pre-pulse is allowed to expand to reduce the density gradient and is subsequently rapidly heated with 7.1 J or 7.3 J pulse of a 0.7 ps FWHM duration for Sm and Gd, respectively. This pump pulse is shaped into a line focus of approximately 30 μm × 9–10 mm FWHM, corresponding to an intensity of $I \sim 3.5$–3.7×10^{15} W cm^{-2} for Sm and Gd, respectively. The target surface was tilted with respect to the axis of the sub-picosecond pulse to define a grazing incidence angle of 35 deg or 43 deg for efficient heating in the case of both Sm and Gd, respectively. To optimize the incidence angle, we changed the angle of the target with respect to the short pulse beam and the position of the grating and charge-couple device (CCD). Due to the short duration of the gain, the mismatch between the propagation velocities of the pump pulse and the amplified pulse significantly reduces the amplification of the x-ray laser pulse. To overcome this limitation, a reflection echelon [15,26] composed of six adjustable mirror segments was used to obtain traveling wave excitation. The traveling wave velocity was adjusted for each new angle, and the focus was corrected for each angle.

Gain measurements were conducted for both the Sm and Gd using single laser shots and moving the targets 1 mm between shots. When the Gd laser was operated at 2.5 Hz repetition rate, the target was translated at a speed of 2.5 mm s^{-1} to renew the surface after each shot. The output of the x-ray lasers was analyzed using a flat-field spectrometer with a nominally 1200 lines/mm variable space grating positioned at a grazing incidence angle of 3 deg and a back-illuminated CCD detector placed at 48 cm from the target. Zirconium filters with a thickness of 2.0 μm were used in the Sm and Gd experiments for target lengths over 4 mm to avoid saturating the detector and to eliminate visible plasma light from reaching the detector. The filter thickness was reduced to 0.5 μm for the measurements with target lengths under 4 mm. In the case of Tb and Dy, we used molybdenum filters with thicknesses of 0.6 μm and 0.3 μm, respectively. The x-ray lasers pulse energies were estimated from the CCD counts taking into account the attenuation of the filters, the grating efficiency, and the quantum efficiency of the detector.

3. RESULTS

Figure 1(a) shows a typical single-shot spectrum of the Ni-like Sm x-ray laser obtained depositing 7.1 J energy of sub-picosecond pulse and 4.3 J of pre-pulse energy on target. Strong amplification is observed in the $4d^1S_0 - 4p^1P_1$ transition at $\lambda = 7.36$ nm (169 eV). The pre-pulse duration was optimized to maximize laser output. Figure 1(b) shows this was found to occur when the pre-pulse has a FWHM duration of ∼185 ps. The delay between the pre-pulse and the sub-picosecond pulse controls the plasma density and density gradient in the gain region, as well as the degree of ionization (fraction of Ni-like ions) at the time of excitation by the sub-picosecond pulse. Figure 1(c) shows that the maximum laser output intensity is observed when the sub-picosecond pulse arrives at the target ∼27 ps after the peak of the 185 ps FWHM pre-pulse. Figure 2 illustrates the Sm x-ray laser intensity grows by more than 3 orders of magnitude as the plasma column length increases from 3 mm to 8 mm. Saturation of the gain is observed to have an onset at a plasma-column length of approximately 5.5 mm. A fit of the data with an expression for the gain that takes into account saturation [27] yields a gain coefficient of 27.3 cm^{-1} with a gain-length product of 16.6. The energy of the most intense Sm laser pulses was estimated to be ∼1.8 μJ from the CCD counts, a value that is sufficient to perform single shot imaging [28].

Similar pre-pulse and sub-picosecond pulse conditions were used to obtain a gain-saturated 6.85 nm (181 eV) laser in Ni-like Gd. Figure 3(a) shows a series of on-axis spectra as a function of the length for a Gd plasma column created by depositing 7.3 J of sub-picosecond pulse energy and 6.9 J of pre-pulse energy on a polished Gd slab target with other irradiation parameters similar to those described above. Figure 3(b) shows the increase in the $\lambda = 6.85$ nm laser line intensity as a function of plasma column length. A fit to the data gives a gain coefficient of 26.3 cm^{-1} and a gain length product of 16.2. The output pulse energy for the longest plasma column length is ∼1 μJ. Weak amplification was also observed for the $\lambda = 6.85$ nm line of Ni-like Sm [see Fig. 1(a)] and in the $\lambda = 6.33$ nm (196 eV) line of Ni-like Gd.

The results were modeled and analyzed with hydrodynamic/atomic physics simulations conducted with the code Radex [29].

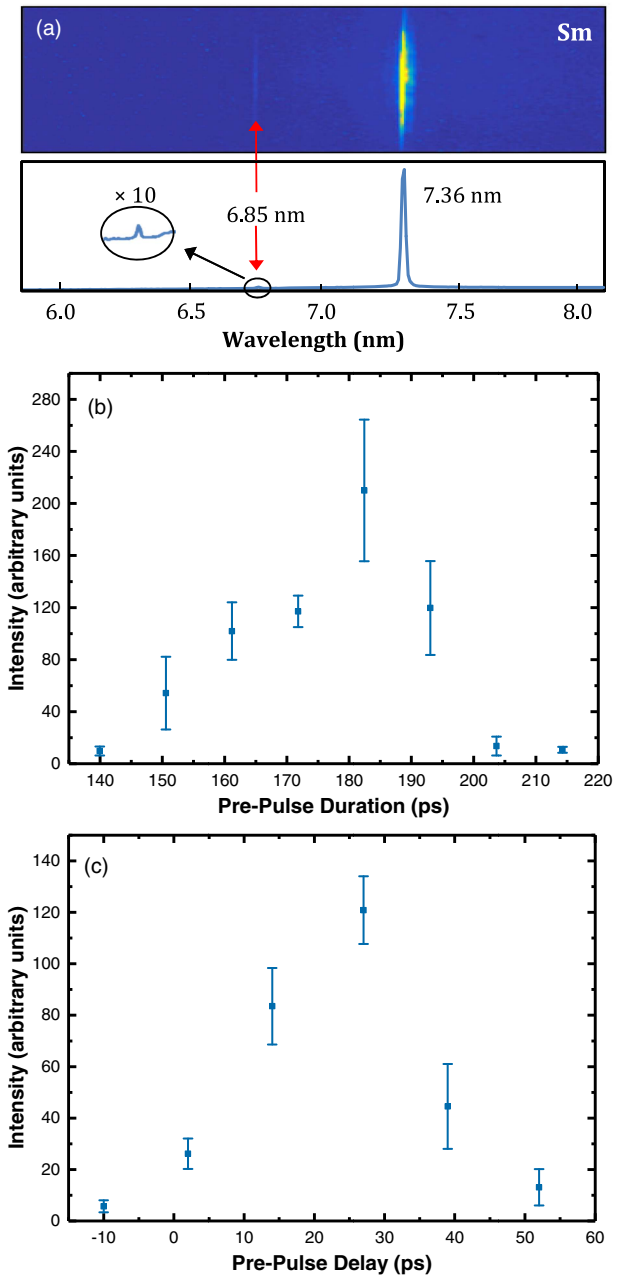

Fig. 1. (a) End-on spectra showing the $\lambda = 7.36$ nm, $4d^1S_0 - 4p^1P_1$ laser line of Ni-like Sm. Insert shows the spectra region near the $\lambda = 6.85$ nm laser line with scale multiplied by 10. (b) Measured $\lambda = 7.36$ nm laser intensity as a function of the pre-pulse duration. The points are the average of several laser shots and the error bar represents one standard deviation. (c) Measured laser intensity as a function of the delay between the peak of the pre-pulse and the peak of the short pulse. The plasma column length was 8 mm corresponding to the target length.

A post-processor ray-tracing code was used to model the soft x-ray laser beam propagation along the plasma column. This allowed us to compute the gain saturation behavior, the role of refraction, the x-ray laser output pulse energy, and the beam divergence. To compute the small signal gain, the Ni-like ions were modeled with 287 levels including all inner and outer shell 3l4l and 3l5l levels, and 2l4l inner shell levels. Other ions in the vicinity of the Ni-like ions were modeled using ~300 single and doubly excited levels

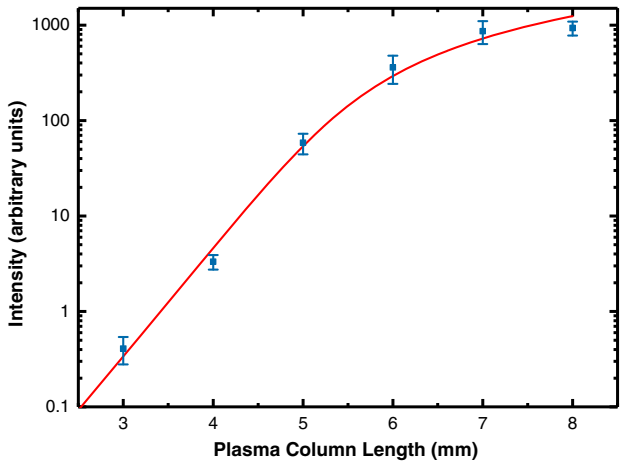

Fig. 2. Intensity of the $\lambda = 7.36$ nm laser line of Ni-like Sm as a function of the plasma-column length. The red line is a fit of the data that yields a gain coefficient of 27.3 cm^{-1} and a gain-length product of 16.6. The error bar represents 1 standard deviation.

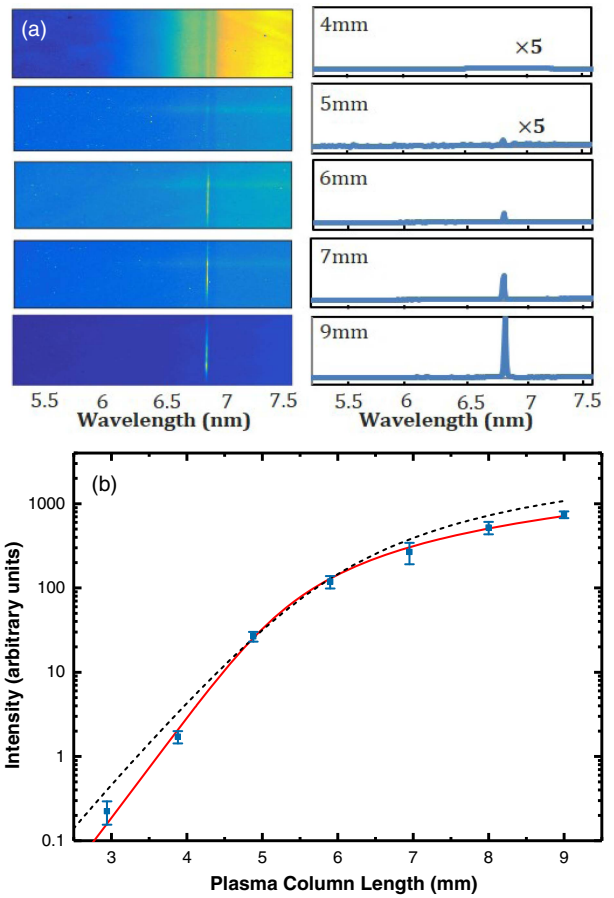

Fig. 3. (a) End-on spectra of a line-focus Gd plasma column showing saturated amplification in the $\lambda = 6.85$ nm line of Ni-like Gd. With the first two integrations plots on the right multiplied by 5. (b) Intensity of the $\lambda = 6.85$ nm laser line as a function of the plasma-column length. The solid red line is a fit of the data that yields a gain coefficient of 26.3 cm^{-1} and a gain-length product of 16.2. The error bar represents 1 standard deviation. The black dashed line is the result of atomic physics/hydrodynamic simulation with a gain-length product of 16.9.

using atomic data and collisional rates from the code HULLAC [30]. Ions far from the Ni-like state were modeled with just the lowest energy outer shell configuration plus the lowest inner shell and double excited levels. The atomic model was run self-consistently with the hydro code including up to 3000 levels. We observed that the computed gain decreases as the complexity of the atomic model and the number of levels is increased until the resulting gain becomes practically insensitive to a further increase in the number of levels. The dashed curve in Fig. 3(b) is the result of the model simulations of the Gd 6.85 nm laser for the pump conditions used in the experiment, assuming the width of the gain region in the direction parallel to the target is 10 μm. Good agreement with the experimental results is observed. The model predicts a beam divergence of 2.4 mrad in the direction parallel to the target, in good agreement with the measured value (Fig. 4). The agreement with the experimental results allows us to use the simulations to further understand the operation of this x-ray laser amplifier. Figure 5 shows the computed spatial distribution of the beam intensity as a function of plasma column length. The model simulations show that in the case of the higher Z-ions, refraction shifts the maximum gain to the lower density region of $4–5 \times 10^{20}$ cm^{-3}. At this density the saturation intensity is computed to be 1.2×10^{10} $W\,cm^{-2}$. Simulations show this intensity is reached after the rays travel ~6 mm along the plasma column axis. The output intensity is computed to exceed the saturation intensity by $>3\times$ at the exit of the amplifier. Refraction is observed to shift the amplified beam progressively away from the target and to decrease the output pulse energy. In the absence of refraction, simulations predict the laser pulse energy would be 5–10 times the amount with refraction, potentially reaching >10 μJ.

The demonstration of a gain-saturated table-top laser at $\lambda = 6.85$ nm in Ni-like Gd at this reduced pump energy also opens the prospect for bright high-repetition-rate plasma-based lasers at shorter wavelengths. In progress toward this goal, we made use of isoelectronic scaling along the elements of the lanthanide series to obtain lasing in several other shorter-wavelength transitions from Ni-like ions. The spectra of Fig. 6 show that the use of similar

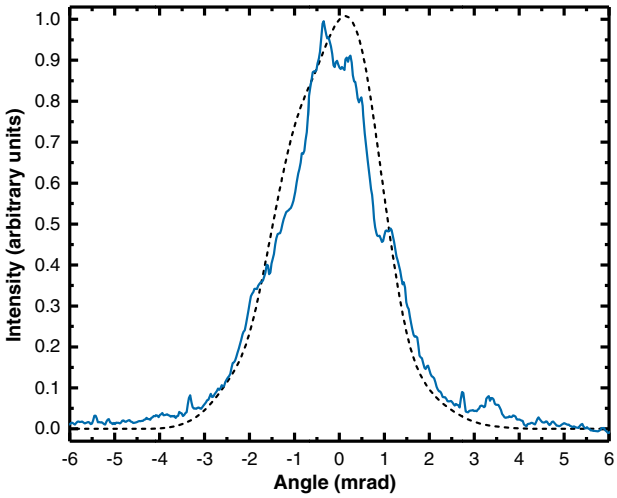

Fig. 4. Measured (blue trace) and simulated (black-dashed trace) Ni-like Gd laser far-field beam intensity profile in the direction parallel to the target surface. The black-dashed line is the modeled far-field intensity. The FWHM beam divergence is ~2.4 mrad.

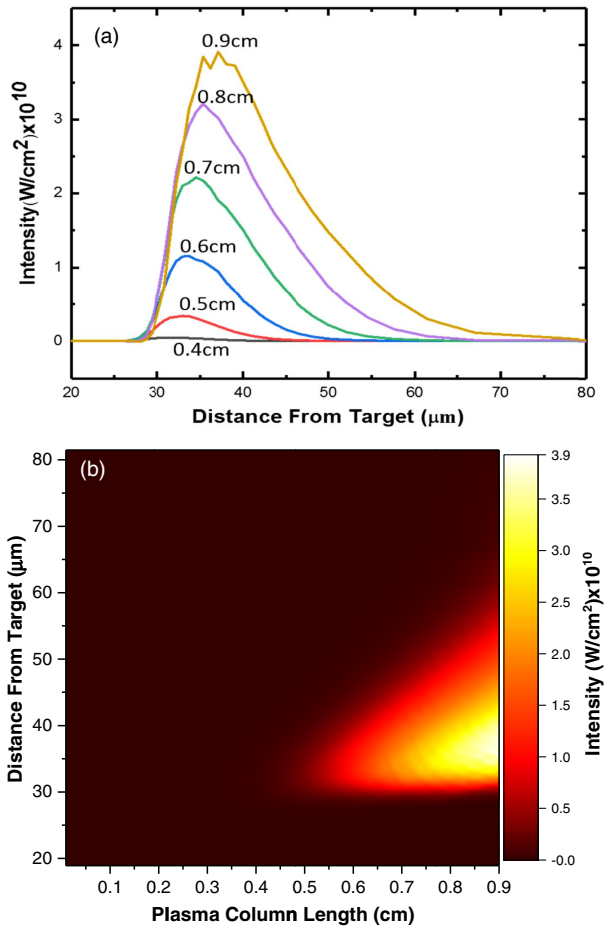

Fig. 5. Computed evolution of the intensity distribution of the x-ray laser beam of the 6.85 nm line of Ni-like Gd as function of plasma column length. (a) Intensity versus distance to the target for increasing plasma column lengths between 0.4 and 0.9 cm. (b) Pseudocolor map of the laser line intensity as a function of distance to the target and plasma column length.

irradiation conditions for Ni-like Gd resulted in strong amplification in the $\lambda = 6.67$ nm (186 eV) and $\lambda = 6.11$ nm (203 eV) transitions of Ni-like Tb. Finally, we have also observed weak amplification in the $\lambda = 5.85$ nm (212 eV) and $\lambda = 6.41$ nm (193 eV) lines of Ni-like Dy (Fig. 6) using the same pump conditions. The limited observed spread of the lines along the vertical direction in the detector, in which length divergence (normal to the dispersion direction) is proportional to the divergence, shows a collimation that is a clear indication of amplification. Another evidence of amplification is the significant shot-to-shot variations of their intensity, indicative of exponential amplification in the non-saturated regime. In all cases, the traveling wave excitation was kept constant and near the speed of light in vacuum. The spectra in Fig. 6 show that the intensity ratio of the longer wavelength to the shorter wavelength of the two $J = 0–1$ lines becomes smaller as Z increases [31], with the shortest wavelength line becoming dominant for Ni-like Dy, as already observed in a normal incidence pumping experiment with much large laser pump energies [12,32].

Another aspect of these amplifiers is the fact that collisional x-ray laser amplification at shorter wavelengths favors higher plasma densities. This is shown by the increase of the grazing

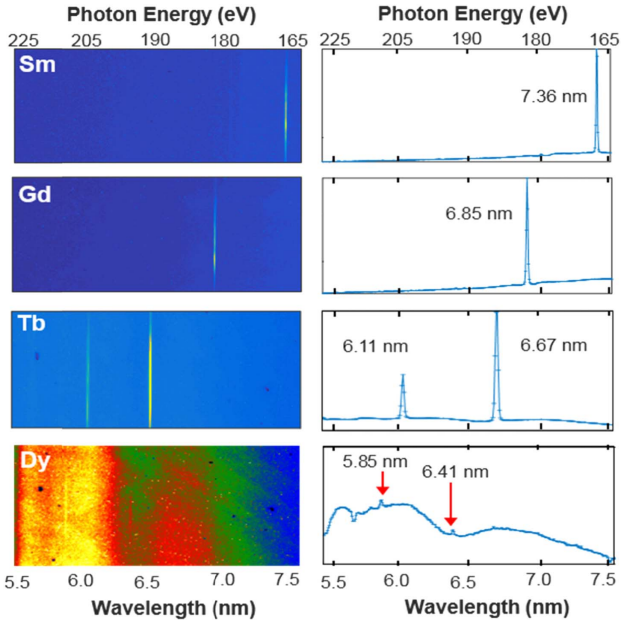

Fig. 6. End-on spectra showing lasing at progressively shorter wavelengths in the $4d^1S_0 - 4p^1P_1$ line of nickel-like lanthanide ions, down to $\lambda = 5.85$ nm in nickel-like Dysprosium.

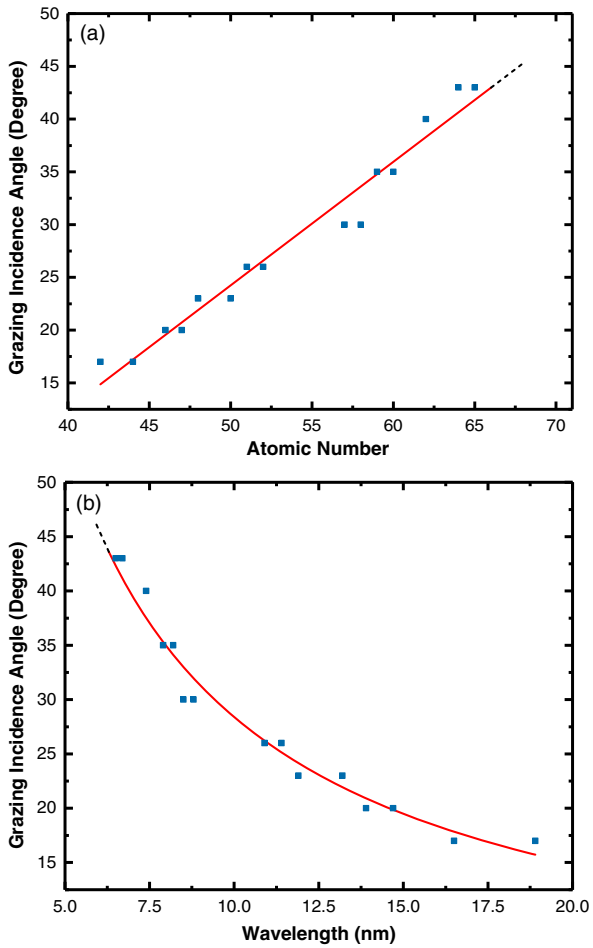

Fig. 7. (a) Measured optimum grazing incidence angle as a function of atomic number. The dashed line is an extrapolation of the data. (b) The optimum grazing incidence angle as a function of lasing wavelength. The dashed line is an extrapolation of the data.

incidence angle of the sub-picosecond pulse necessary for optimum laser amplification, which is related to the electron density at which the pump rays refract [33]. Combining the experimental data of the optimum pump incidence angle obtained in this work with our previously published data for grazing incidence pumping for lasing in lower Z Ni-like ions [17,18,22,34], it is possible to experimentally map the dependence of the optimum pump angle and plasma density for a large range of Z and lasing wavelengths. This provides both a benchmark for simulation codes as well as a prediction of the optimum condition for further scaling these lasers to shorter wavelengths. The increase in irradiation angle is observed to be linear over a broad range of atomic numbers ranging from $Z = 42$ (Mo) to $Z = 66$ (Dy) (Fig. 7). In this range of Z, the optimum picosecond or sub-picosecond pulse irradiation angle is observed to increase from a grazing incidence angle of ~17 deg for Mo to 43 deg for Dy. This corresponds to an increase in electron density from 1.5×10^{20} cm^{-3} to 8×10^{20} cm^{-3}. As discussed above, the model simulations show that in the case of the higher Z-ions refraction shifts the maximum gain to the lower-density region.

4. CONCLUSION

In conclusion, we have extended compact gain-saturated plasma-based lasers to the shortest wavelength to date: 6.85 nm. We have also observed laser amplification in other Ni-like lanthanide ions at wavelengths as short as 5.85 nm, opening the possibility of scaling table-top gain-saturated lasers to even shorter wavelengths. The optimum sub-picosecond pulse irradiation angle for the excitation of transient gain-saturated Ni-like x-ray lasers was determined from experimental measurements to increase linearly for elements ranging from $Z = 42$ to $Z = 66$. The results will make possible applications requiring bright laser pulses with a large number of photons at these short wavelengths, such as single-shot ultra-high-resolution imaging of dynamic nano-scale phenomena to be realized at compact facilities.

Funding. U.S. Department of Energy (DOE), Office of Science (SC), Basic Energy Sciences (BES) (DE-FG02-04ER15592).

Acknowledgment. We acknowledge the use of the CU-CSU Summit Computer Facility to conduct the simulations, NSF (ACI-1532235). M. Berrill acknowledges Oak Ridge National Laboratory. This paper has been authored by UT-Battelle, LLC, under contract DE-AC05-00OR22725 with the U.S. Department of Energy (DOE).

REFERENCES

1. B. W. J. McNeil and N. R. Thompson, "X-ray free-electron lasers," Nat. Photonics **4**, 814–821 (2010).
2. Kuznetsov, J. Filevich, F. Dong, M. Woolston, W. L. Chao, E. H. Anderson, E. R. Bernstein, D. C. Crick, J. J. Rocca, and C. S. Menoni, "Three-dimensional nanoscale molecular imaging by extreme ultraviolet laser ablation mass spectrometry," Nat. Commun. **6**, 6944 (2015).
3. G. Vaschenko, C. Brewer, F. Brizuela, Y. Wang, M. A. Larotonda, B. M. Luther, M. C. Marconi, J. J. Rocca, C. S. Menoni, E. H. Anderson, W. Chao, B. D. Harteneck, J. A. Liddle, Y. Liu, and D. T. Attwood, "Sub-38 nm resolution tabletop microscopy with 13 nm wavelength laser light," Opt. Lett. **31**, 1214–1216 (2006).

4. R. F. Smith, J. Dunn, J. Nilsen, V. N. Shlyaptsev, S. Moon, J. Filevich, J. J. Rocca, M. C. Marconi, J. R. Hunter, and T. W. Barbee, Jr., "Picosecond X-ray laser interferometry of dense plasmas," Phys. Rev. Lett. **89**, 065004 (2002).
5. F. Brizuela, S. Carbajo, A. Sakdinawat, D. Alessi, D. H. Martz, Y. Wang, B. Luther, K. A. Goldberg, I. Mochi, D. T. Attwood, B. La Fontaine, J. J. Rocca, and C. S. Menoni, "Extreme ultraviolet laser-based table-top aerial image metrology of lithographic masks," Opt. Express **18**, 14467 (2010).
6. R. Z. Tai, K. Namikawa, M. Kishimoto, M. Tanaka, K. Sukegawa, N. Hasegawa, T. Kawachi, M. Kado, P. Lu, K. Nagashima, H. Daido, H. Maruyama, A. Sawada, M. Ando, and Y. Kato, "Picosecond snapshot of the speckles from ferroelectric $BaTiO_3$ by means of x-ray lasers," Phys. Rev. Lett. **89**, 257602 (2002).
7. L. M. Meng, D. Alessi, O. Guilbaud, Y. Wang, M. Berrill, B. M. Luther, S. R. Domingue, D. H. Martz, D. Joyeux, S. De Rossi, J. J. Rocca, and A. Klisnick, "Temporal coherence and spectral linewidth of an injection-seeded transient collisional soft x-ray laser," Opt. Express **36**, 2164 (2011).
8. Ph. Zeitoun, G. Faivre, S. Sebban, T. Mocek, A. Hallou, M. Fajardo, D. Aubert, Ph. Balcou, F. Burgy, D. Douillet, S. Kazamias, G. de Lachèze-Murel, T. Lefrou, S. le Pape, P. Mercère, H. Merdji, A. S. Morlens, J. P. Rousseau, and C. Valentin, "A high-intensity highly coherent soft X-ray femtosecond laser seeded by a high harmonic beam," Nature **431**, 426–429 (2004).
9. Y. Wang, E. Granados, F. Pedaci, D. Alessi, B. Luther, M. Berrill, and J. J. Rocca, "Phase-coherent, injection-seeded, table-top soft-X-ray lasers at 18.9 nm and 13.9 nm," Nat. Photonics **2**, 94–98 (2008).
10. Y. Wang, L. Yin, S. Wang, M. C. Marconi, J. Dunn, E. Gullikson, and J. J. Rocca, "Single-shot soft X-ray laser linewidth measurement using a grating interferometer," Opt. Lett. **38**, 5004–5007 (2013).
11. J. J. Rocca, "Table-top soft X-ray lasers," Rev. Sci. Instrum. **70**, 3799–3827 (1999).
12. R. Smith, G. J. Tallents, J. Zhang, G. Eker, S. McCabe, G. J. Pert, and E. Wolfrum, "Saturation behavior of two x-ray lasing transitions in Ni-like Dy," Phys. Rev. A **59**, R47 (1999).
13. J. Zhang, A. G. MacPhee, J. Lin, E. Wolfrum, R. Smith, C. Danson, M. H. Key, C. L. S. Lewis, D. Neely, J. Nilsen, G. J. Pert, G. J. Tallents, and J. S. Wark, "A saturated x-ray laser beam at 7 nanometers," Science **276**, 1097–1100 (1997).
14. P. V. Nickles, V. N. Shlyaptsev, M. Kalachnikov, M. Schnurer, I. Will, and W. Sandner, "Short pulse x-ray laser at 32.6 nm based on transient gain in Ne-like titanium," Phys. Rev. Lett. **78**, 2748–2751 (1997).
15. J. Dunn, Y. Li, A. L. Osterheld, J. Nilsen, J. R. Hunter, and V. N. Shlyaptsev, "Gain saturation regime for tabletop, Ni-Like ion transient x-ray lasers," Phys. Rev. Lett. **84**, 4834–4837 (2000).
16. R. Keenan, J. Dunn, P. K. Patel, D. F. Price, R. F. Smith, and V. N. Shlyaptsev, "High-repetition-rate grazing- incidence pumped x-ray laser operating at 18.9 nm," Phys. Rev. Lett. **94**, 103901 (2005).
17. B. M. Luther, Y. Wang, M. A. Larotonda, D. Alessi, M. Berrill, M. C. Marconi, J. J. Rocca, and V. N. Shlyaptsev, "Saturated high-repitition-rate 18.9-nm tabletop laser in nickellike molybdenum," Opt. Lett. **30**, 165–167 (2005).
18. Y. Wang, M. A. Larotonda, B. M. Luther, D. Alessi, M. Berrill, V. N. Shlyaptsev, and J. J. Rocca, "Demonstration of high-repetition-rate tabletop soft-x-ray lasers with saturated output at wavelengths down to 13.9 nm and gain down to 10.9 nm," Phys. Rev. A **72**, 053807 (2005).
19. B. A. Reagan, M. Berrill, K. A. Wernsing, C. Baumgarten, M. Woolston, and J. J. Rocca, "High-average-power, 100-Hz repetition-rate, tabletop soft-x-ray lasers at sub-15-nm wavelengths," Phys. Rev. A **89**, 053820 (2014).
20. C. Baumgarten, M. Pedicone, H. Bravo, H. Wang, L. Yin, C. S. Menoni, J. J. Rocca, and B. A. Reagan, "1 J, 0.5 kHz repetition rate picosecond laser," Opt. Lett. **41**, 3339–3342 (2016).
21. D. Alessi, Y. Wang, D. Martz, B. Luther, L. Yin, D. H. Martz, M. R. Woolston, Y. Liu, M. Berrill, and J. J. Rocca, "Efficient excitation of gain-saturated sub-9 nm wavelength table-top soft X-ray lasers and lasing down to 7.36 nm," Phys. Rev. X **1**, 021023 (2011).
22. J. E. Balmer, F. Staub, and F. Jia, "Soft-X-ray lasing down to 6.85 nm in Ni-like samarium," in *Springer Proceedings in Physics* (2014), Vol. **147**, Chap. 5.
23. H. Daido, Y. Kato, K. Murai, S. Ninomiya, R. Kodame, G. Yuan, Y. Oshikane, M. Takagi, H. Takabe, and F. Koike, "Efficient soft x-ray lasing at 6–8 nm in nickel-like lanthanides," Phys. Rev. Lett. **75**, 1074–1077 (1995).
24. Y. Luo, A. Morozov, D. Gordon, P. Sprangle, A. Svidzinshy, H. Xia, M. Scully, and S. Suckewer, "Possibility of recombination gain increase in CV ions at 4.0 nm via coherence," in *Springer Proceedings in Physics* (2016), vol. **169**, pp. 21–33.
25. Y. Wang, S. Wang, A. Rockwood, B. M. Luther, R. Hollinger, A. Curtis, C. Calvi, C. S. Menoni, and J. J. Rocca, "0.85 PW laser operation at 3.3 Hz and high-contrast ultrahigh-intensity $\lambda = 400$ nm second-harmonic beamline," Opt. Lett. **42**, 3828–3831 (2017).
26. J. R. Crespo Lopez-Urrutia and E. E. Fill, "Traveling-wave excitation of an x-ray laser medium," Proc. SPIE **2012**, 258 (1994).
27. G. J. Tallents, Y. Abou-Ali, M. Edwards, R. E. King, G. J. Pert, S. J. Pestehe, F. Strati, R. Keenan, C. L. S. Lewis, S. Topping, O. Guilbaud, A. Klisnick, D. Ros, R. Clarke, D. Neely, and M. Notley, *X-Ray Lasers 2002: 8th International Conference on X-Ray Lasers*, J. J. Rocca, J. Dunn, and S. Suckewer, eds., AIP Conference Proceedings, No. C641 (AIP, 2002), p. 291.
28. M.-C. Chou, R.-P. Huang, P.-H. Lin, C.-T. Huang, S.-Y. Chen, H.-H. Chu, J. Wang, and J.-Y. Lin, "Single-shot soft-x-ray digital holographic microscopy with an adjustable field of view and magnification," Opt. Lett. **34**, 623–625 (2009).
29. A. V. Vinogradov and V. N. Shlyaptsev, "Characteristics of a laser plasma x-ray source (review)," Sov. J. Quantum Electron. **17**, 1–14 (1987).
30. A. Bar-Shalom, M. Klapisch, and J. Oreg, "Hullac, an integrated computer package for atomic processes in plasmas," J. Quantum Spectrosc. Radiat. Transfer **71**, 169–188 (2001).
31. B. J. MacGowan, L. B. Da Silva, D. J. Fields, C. J. Keane, J. A. Koch, R. A. London, D. L. Matthews, S. Maxon, S. Mrowka, A. L. Osterheld, J. H. Scofield, G. Shimkaveg, J. E. Trebes, and R. S. Walling, "Short wavelength x-ray laser research at the Lawrence Livermore National Laboratory," Phys. Fluids B **4**, 2326–2337 (1992).
32. H. Daido, "Review of soft x-ray laser researches and developments," Rep. Prog. Phys. **65**, 1513–1576 (2002).
33. R. A. London, "Beam optics of exploding foil plasma x-ray lasers," Phys. Fluids **31**, 184–192 (1988).
34. M. A. Larotonda, B. M. Luther, Y. Wang, Y. Liu, D. Alessi, M. Berrill, A. Dummer, F. Brizuela, C. S. Menoni, M. C. Marconi, V. N. Shlyaptsev, J. Dunn, and J. J. Rocca, "Characteristics of a saturated 18.9-nm tabletop laser operating at 5-Hz repetition rate," IEEE J. Sel. Top. Quantum Electron. **10**, 1363–1367 (2004).